Turk. J. Math. Comput. Sci.
17(2)(2025) 378–395

DOI : 10.47000/tjmcs.1696188

Exploring the Dynamics of Measles Infection: A Fractional Calculus Approach to Stochastic Modeling

Mehmet Akif Çetin[1], Seda İğret Araz[2,*]

[1]*ALTSO Vocational School, Alanya Alaaddin Keykubat University, 7400, Antalya, Turkey.*
[2]*Department of Mathematics Education, Faculty of Education, Siirt University, 56100, Siirt, Turkey.*

Received: 09-05-2025 • Accepted: 10-07-2025

Abstract. This article develops and analyzes a measles infection model using fractional calculus and stochastic methods. The existence and uniqueness of solutions are proven by verifying linear growth and Lipschitz conditions. The model, formulated with the Caputo fractional derivative, is numerically solved via the Newton polynomial method. Simulations illustrate the dynamics of measles infections, offering valuable theoretical and numerical insights that enhance understanding of infectious disease modeling.

2020 AMS Classification: 92C60, 26A33, 60H10

Keywords: Measles infection, fractional order, stochastic framework, Caputo fractional derivative.

1. Introduction

Mathematical epidemiology employs mathematical models to understand the dynamics of infectious disease spread and to devise effective control strategies. Classical compartmental models—such as SIR and SEIR—typically rely on integer-order derivatives, which describe how the system evolves based solely on its current state and instantaneous rate of change [3, 6, 8, 12]. However, in real-world scenarios, particularly in the spread of infectious diseases, memory effects and the influence of past states are significant. This is where fractional calculus becomes relevant. Fractional derivatives generalize classical differentiation to non-integer (fractional) orders, allowing the derivative order to take any real value, often between 0 and 1. Unlike integer-order derivatives, fractional derivatives incorporate memory effects, meaning they consider not only the current rate of change but also the cumulative impact of the system's past behavior. This feature makes them particularly well-suited for modeling biological processes with inherent delays, such as incubation periods, immune responses, and delayed interventions like quarantine or vaccination.

In this context, fractional-order models more effectively capture the long-term dependencies and delayed effects that classical models may overlook. Disease transmission in real populations is rarely smooth or instantaneous. Instead, it often exhibits irregular and heterogeneous patterns due to variations in age, mobility, immunity, and social behavior. Fractional models can more accurately represent such heterogeneity and complexity. Furthermore, they provide more reliable long-term forecasts and risk assessments, including the potential for disease resurgence after an outbreak. For examples of existing fractional-order epidemic models, the reader is referred to [2, 4, 7, 9, 13, 15]. In addition to fractional models, stochastic models are another essential tool in mathematical epidemiology. These models explicitly incorporate randomness and uncertainty in the transmission process. Since real-world epidemics involve unpredictable

*Corresponding Author
Email addresses: akif.cetin@alanya.edu.tr (M.A. Çetin), sedaaraz@siirt.edu.tr (S. İğret Araz)

elements such as random contacts, individual immune variability, and environmental fluctuations, stochastic modeling offers a more realistic representation of epidemic behavior. In stochastic models, events like infection, recovery, and death occur according to probability distributions. Importantly, a disease may fail to spread below a certain threshold in a deterministic model but still cause an outbreak due to random fluctuations. Stochastic effects are especially significant in small populations, where chance events have a greater impact. These models are particularly useful for estimating outbreak probabilities, evaluating the effectiveness of quarantine and vaccination strategies, and analyzing the influence of travel restrictions. For related work on measles outbreaks modeled stochastically, see [10, 11, 14].

Before proceeding to the next section, we introduce the definitions of the Caputo fractional derivative and the fractional integral with a power-law kernel, both of which will be utilized in our analysis. The Caputo fractional derivative [5] of a function $\upsilon(t) \in H^1(0,T)$ is defined as follows:

$$ {}_0^C D_t^\alpha \upsilon(t) = \frac{1}{\Gamma(1-\alpha)} \int_0^t \frac{d}{d\tau} \upsilon(\tau) (t-\tau)^{-\alpha} \, d\tau, $$

and the fractional integral of the function $\upsilon(t)$ is given as follows

$$ {}_0 I_t^\alpha \upsilon(t) = \frac{1}{\Gamma(\alpha)} \int_0^t \upsilon(\tau) (t-\tau)^{\alpha-1} \, d\tau. $$

2. Model Formulation

Measles remains one of the most contagious infectious diseases, with serious health consequences, particularly in populations with low vaccination coverage. Despite the widespread availability of effective vaccines, outbreaks continue to occur globally, posing a persistent threat to public health. A thorough understanding of measles transmission dynamics and control measures is essential for preventing large-scale outbreaks and reducing associated morbidity and mortality. Mathematical modeling serves as a powerful tool for analyzing the spread of measles, assessing the effectiveness of vaccination programs, and evaluating the potential impact of various public health interventions. By developing accurate and robust models, researchers can predict the progression of outbreaks, assess the efficacy of control strategies, and inform policy decisions aimed at achieving herd immunity and preventing future epidemics. In this section, we present a measles infection model introduced in [1], formulated as follows:

$$ \begin{aligned} \dot{S} &= \omega + \tau V - (b + \rho + \beta I) S, \\ \dot{E} &= \beta I S - (\rho + \mu) E, \\ \dot{V} &= bS - (\rho + \tau) V, \\ \dot{I} &= \mu E - (\psi + \rho + \eta + \theta) I, \\ \dot{Q} &= \eta I - (c + \rho + \delta) Q, \\ \dot{R} &= \theta I + \delta Q - \rho R, \end{aligned} \tag{2.1} $$

where transmission coefficient is $\beta = \varpi \frac{K}{N}$. Here ϖ denotes the probability of infection upon contact and K represents the contact rate with $0 < K < 1$. The initial conditions are

$$ S(0) = S_0, \; E(0) = E_0, \; V(0) = V_0, \; I(0) = I_0, \; Q(0) = Q_0, \; R(0) = R_0. $$

In the model (2.1), the total human population is divided into six classes. The function $S(t)$ represents the number of susceptible individuals at time t, the function $E(t)$ represents the number of exposed individuals (infected but not yet infectious) at time t, the function $V(t)$ expresses the number of vaccinated individuals at time t, the function $I(t)$ is the number of infectious individuals at time t, the function $Q(t)$ is the number of infected individuals who are quarantined at time t and the function $R(t)$ describes the number of recovered individuals at time t. On the other hand, the meaning of the parameters on the right side of model (2.1) is as follows: ω is recruitment rate, τ is immunity decay rate, b is the rate at which susceptible is vaccinated, ρ is natural mortality rate, β is the rate of infection per contact between susceptibles and infectives, μ is the rate of progression of E class to I class, ψ is the mortality rate of I due to measles

disease, η is the rate at which infected persons are isolated, θ is the recovery rate of I following treatment, c is the mortality rate of Q due to measles disease and δ is the recovery rate of Q following treatment.

3. Stochastic Model of Measles Infection

In this section, we introduce a stochastic version of the classical measles model to capture the randomness in disease dynamics. Using the linear growth assumption and verifying the Lipschitz condition, we prove the existence and uniqueness of the solution. The linear growth ensures bounded behavior, while the Lipschitz condition guarantees a unique and stable solution, providing a rigorous foundation for the model's validity under stochastic influences [3]. In this section, we consider the following stochastic measles infection model:

$$\begin{aligned}
dS\,(t) &= [\omega + \tau V - (b + \rho + \beta I)\,S\,]\,dt + \sigma_1 S\,(t)\,dB_1\,(t)\,,\\
dE\,(t) &= [\beta IS\, - (\rho + \mu)\,E]\,dt + \sigma_2 E\,(t)\,dB_2\,(t)\,,\\
dV\,(t) &= [bS - (\rho + \tau)\,V]\,dt + \sigma_3 V\,(t)\,dB_3\,(t)\,,\\
dI\,(t) &= [\mu E - (\psi + \rho + \eta + \theta)\,I]\,dt + \sigma_4 I\,(t)\,dB_4\,(t)\,,\\
dQ\,(t) &= [\eta I - (c + \rho + \delta)\,Q]\,dt + \sigma_5 Q\,(t)\,dB_5\,(t)\,,\\
dR\,(t) &= [\theta I + \delta Q - \rho R]\,dt + \sigma_6 R\,(t)\,dB_6\,(t)\,,
\end{aligned} \tag{3.1}$$

where σ_i, $i = 1, ..., 6$ is the intensity of the noise affecting each population and $B_i\,(t)$ is standard Wiener process (Brownian motion) representing random fluctuation.

In real-world problems, biological and social processes can be inherently stochastic due to various sources of variability. Environmental factors, including seasonal fluctuations and climatic conditions, can introduce temporal heterogeneity in disease transmission. Moreover, the frequency and nature of contacts between individuals can occur in a random manner, contributing to transmission uncertainty. Demographic events such as births, deaths, and migration are also subject to unpredictable variations. Additionally, heterogeneity in vaccination effectiveness and compliance further complicates the dynamics of population immunity. Deterministic models, which assume constant and predictable rates, may therefore inadequately capture these complexities, potentially oversimplifying the underlying epidemic processes. To address these inherent natural random fluctuations, we will proceed by extending and analyzing the deterministic model through the inclusion of stochastic components.

3.1. Existence and Uniqueness of the Model.

In this subsection, we rewrite the system (3.1) as follows

$$\begin{aligned}
dS\,(t) &= u_1\,(t, S)\,dt + C_1\,(t, S)\,dB_1\,(t)\,,\\
dE\,(t) &= u_2\,(t, E)\,dt + C_2\,(t, E)\,dB_2\,(t)\,,\\
dV\,(t) &= u_3\,(t, V)\,dt + C_3\,(t, V)\,dB_3\,(t)\,,\\
dI\,(t) &= u_4\,(t, I)\,dt + C_4\,(t, I)\,dB_4\,(t)\,,\\
dQ\,(t) &= u_5\,(t, Q)\,dt + C_5\,(t, Q)\,dB_5\,(t)\,,\\
dR\,(t) &= u_6\,(t, R)\,dt + C_6\,(t, R)\,dB_6\,(t)\,.
\end{aligned}$$

Before proceeding with the proof, we shall define the following notations:

$$X_i = \begin{bmatrix} S \\ E \\ V \\ I \\ Q \\ R \end{bmatrix}, C_i\,(t, X_i) = \sigma_i X_i\,\{i = 1, ..., 6\}\,.$$

To achieve our aim, we need to show that linear growth condition and the Lipschitz condition are satisfied [3], i.e.,

$$|u_i\,(t, X_i)|^2\,,\ \ |C_i\,(t, X_i)|^2 < l_i\left(1 + |X_i|^2\right)$$

and

$$\left|u_i\left(t, X_i^1\right) - u_i\left(t, X_i^2\right)\right|,\ \ \left|C_i\left(t, X_i^1\right) - C_i\left(t, X_i^2\right)\right| \leq \bar{l}_i\left|X_i^1 - X_i^2\right|^2.$$

Firstly, we will prove the the linear growth condition. For the function $u_1(t,S)$:

$$\begin{aligned}
|u_1(t,S)|^2 &= |\omega + \tau V - (b+\rho+\beta I)S|^2 \\
&\leq 3\left[\omega^2 + \tau^2|V|^2 + (b+\rho+\beta I)^2|S|^2\right] \\
&\leq 3\left[\omega^2 + \tau^2|V|^2 + \left(3b^2+3\rho^2+3\beta^2|I|^2\right)|S|^2\right] \\
&\leq 3\left[\omega^2 + \tau^2 \sup_{0\leq t\leq T}|V|^2 + \left(3b^2+3\rho^2+3\beta^2 \sup_{0\leq t\leq T}|I|^2\right)|S|^2\right] \\
&\leq 3\left[\omega^2 + \tau^2\left\|V^2\right\|_\infty + \left(3b^2+3\rho^2+3\beta^2\left\|I^2\right\|_\infty\right)|S|^2\right] \\
&\leq 3\left(\omega^2 + \tau^2\left\|V^2\right\|_\infty\right)\left[1 + m_1|S|^2\right],
\end{aligned}$$

where

$$m_1 = \frac{3b^2+3\rho^2+3\beta^2\left\|I^2\right\|_\infty}{\omega^2+\tau^2\left\|V^2\right\|_\infty} < 1.$$

Then

$$|u_1(t,S)|^2 \leq l_1\left(1+|S|^2\right).$$

For the function $u_2(t,E)$:

$$\begin{aligned}
|u_2(t,E)|^2 &= |\beta IS - (\rho+\mu)E|^2 \\
&\leq 2\left[\beta^2 I^2|S|^2 + (\rho+\mu)^2|E|^2\right] \\
&\leq 2\left[\beta^2 I^2 \sup_{0\leq t\leq T}|S|^2 + (\rho+\mu)^2|E|^2\right] \\
&\leq 2\left[\beta^2 I^2\left\|S^2\right\|_\infty + \left(2\rho^2+2\mu^2\right)|E|^2\right] \\
&\leq 2\beta^2 I^2\left\|S^2\right\|_\infty\left[1+m_2|E|^2\right],
\end{aligned}$$

where

$$m_2 = \frac{2\rho^2+2\mu^2}{\beta^2 I^2\left\|S^2\right\|_\infty} < 1.$$

Then

$$|u_2(t,E)|^2 \leq l_2\left(1+|E|^2\right).$$

For the function $u_3(t,V)$:

$$\begin{aligned}
|u_3(t,V)|^2 &= |bS - (\rho+\tau)V|^2 \\
&\leq 2\left[b^2|S|^2 + (\rho+\tau)^2|V|^2\right] \\
&\leq 2\left[b^2 \sup_{0\leq t\leq T}|S|^2 + (\rho+\tau)^2|V|^2\right] \\
&\leq 2\left[b^2\left\|S^2\right\|_\infty + \left(2\rho^2+2\tau^2\right)|V|^2\right] \\
&\leq 2b^2\left\|S^2\right\|_\infty\left[1+m_3|V|^2\right],
\end{aligned}$$

where

$$m_3 = \frac{2\rho^2+2\tau^2}{b^2\left\|S^2\right\|_\infty} < 1.$$

Then

$$|u_3(t,V)|^2 \leq l_3\left(1+|V|^2\right).$$

For the function $u_4(t, I)$:

$$\begin{aligned}
|u_4(t,I)|^2 &= |\mu E - (\psi+\rho+\eta+\theta) I|^2 \\
&\leq 2\left[\mu^2 |E|^2 + (\psi+\rho+\eta+\theta)^2 |I|^2\right] \\
&\leq 2\left[\mu^2 \sup_{0\leq t\leq T} |E|^2 + (\psi+\rho+\eta+\theta)^2 |I|^2\right] \\
&\leq 2\left[\mu^2 \left\|E^2\right\|_\infty + 4\left(\psi^2+\rho^2+\eta^2+\theta^2\right)|I|^2\right] \\
&\leq 2\mu^2 \left\|E^2\right\|_\infty \left[1 + m_4 |I|^2\right]
\end{aligned}$$

where

$$m_4 = \frac{4\left(\psi^2+\rho^2+\eta^2+\theta^2\right)}{\mu^2 \left\|E^2\right\|_\infty} < 1.$$

Then,

$$|u_4(t,I)|^2 \leq l_4\left(1+|I|^2\right).$$

For the function $u_5(t, Q)$:

$$\begin{aligned}
|u_5(t,Q)|^2 &= |\eta I - (c+\rho+\delta) Q|^2 \\
&\leq 2\left[\eta^2 |I|^2 + (c+\rho+\delta)^2 |Q|^2\right] \\
&\leq 2\left[\eta^2 \sup_{0\leq t\leq T} |I|^2 + (c+\rho+\delta)^2 |Q|^2\right] \\
&\leq 2\left[\eta^2 \left\|I^2\right\|_\infty + 3\left(c^2+\rho^2+\delta^2\right)|Q|^2\right] \\
&\leq 2\eta^2 \left\|I^2\right\|_\infty \left[1 + m_5 |Q|^2\right],
\end{aligned}$$

where

$$m_5 = \frac{3\left(c^2+\rho^2+\delta^2\right)}{\eta^2 \left\|I^2\right\|_\infty} < 1.$$

Then,

$$|u_5(t,Q)|^2 \leq l_5\left(1+|Q|^2\right).$$

For the function $u_6(t, R)$:

$$\begin{aligned}
|u_6(t,R)|^2 &= |\theta I + \delta Q - \rho R|^2 \\
&\leq 3\left[\theta^2 |I|^2 + \delta^2 |Q|^2 + \rho^2 |R|^2\right] \\
&\leq 3\left[\theta^2 \sup_{0\leq t\leq T} |I|^2 + \delta^2 \sup_{0\leq t\leq T} |Q|^2 + \rho^2 |R|^2\right] \\
&\leq 3\left[\theta^2 \left\|I^2\right\|_\infty + \delta^2 \left\|Q^2\right\|_\infty + \rho^2 |R|^2\right] \\
&\leq 3\left(\theta^2 \left\|I^2\right\|_\infty + \delta^2 \left\|Q^2\right\|_\infty\right)\left[1 + m_6 |R|^2\right],
\end{aligned}$$

where

$$m_6 = \frac{\rho^2}{\theta^2 \left\|I^2\right\|_\infty + \delta^2 \left\|Q^2\right\|_\infty} < 1.$$

Then,

$$|u_6(t,R)|^2 \leq l_6\left(1+|R|^2\right).$$

On the other hand, for the stochastic part we write

$$\begin{aligned}
|C_1(t,S)|^2 &= \sigma_1^2 |S|^2 \leq \sigma_1^2 \left(1+|S|^2\right),\\
|C_2(t,E)|^2 &= \sigma_2^2 |E|^2 \leq \sigma_2^2 \left(1+|E|^2\right),\\
|C_3(t,V)|^2 &= \sigma_3^2 |V|^2 \leq \sigma_3^2 \left(1+|V|^2\right),\\
|C_4(t,I)|^2 &= \sigma_4^2 |I|^2 \leq \sigma_4^2 \left(1+|I|^2\right),\\
|C_5(t,Q)|^2 &= \sigma_5^2 |Q|^2 \leq \sigma_5^2 \left(1+|Q|^2\right),\\
|C_6(t,R)|^2 &= \sigma_6^2 |R|^2 \leq \sigma_6^2 \left(1+|R|^2\right).
\end{aligned}$$

Thus, we verified the linear growth condition [3] under the condition that:

$$\max\{m_1, m_2, m_3, m_4, m_5, m_6\} < 1.$$

Now, we prove the Lipschitz condition:

$$\begin{aligned}
\left|u_1\left(t,S^1\right)-u_1\left(t,S^2\right)\right|^2 &= \left|(-b-\rho-\beta I)\left(S^1-S^2\right)\right|^2\\
&\leq 3\left|b^2+\rho^2+\beta^2|I|^2\right|\left|S^1-S^2\right|^2\\
&\leq 3\left|b^2+\rho^2+\beta^2\sup_{0\leq t\leq T}|I|^2\right|\left|S^1-S^2\right|^2\\
&\leq 3\left|b^2+\rho^2+\beta^2\left\|I^2\right\|_\infty\right|\left|S^1-S^2\right|^2\\
&= \bar{l}_1\left|S^1-S^2\right|^2,\\
\left|u_2\left(t,E^1\right)-u_2\left(t,E^2\right)\right|^2 &= \left|-(\rho+\mu)\left(E^1-E^2\right)\right|^2\\
&\leq \left|\varepsilon_1^2+(\rho+\mu)^2\right|\left|E^1-E^2\right|^2\\
&= \bar{l}_2\left|E^1-E^2\right|^2,\\
\left|u_3\left(t,V^1\right)-u_3\left(t,V^2\right)\right|^2 &= \left|-(\rho+\tau)\left(V^1-V^2\right)\right|^2\\
&\leq \left|\varepsilon_2^2+(\rho+\tau)^2\right|\left|V^1-V^2\right|^2\\
&= \bar{l}_3\left|V^1-V^2\right|^2,\\
\left|u_4\left(t,I^1\right)-u_4\left(t,I^2\right)\right|^2 &= \left|-(\psi+\rho+\eta+\theta)\left(I^1-I^2\right)\right|^2\\
&\leq \left|\varepsilon_3^2+(\psi+\rho+\eta+\theta)^2\right|\left|I^1-I^2\right|^2\\
&= \bar{l}_4\left|I^1-I^2\right|^2,\\
\left|u_5\left(t,Q^1\right)-u_5\left(t,Q^2\right)\right|^2 &= \left|-(c+\rho+\delta)\left(Q^1-Q^2\right)\right|^2\\
&\leq \left|\varepsilon_4^2+(c+\rho+\delta)^2\right|\left|Q^1-Q^2\right|^2\\
&= \bar{l}_5\left|Q^1-Q^2\right|^2,\\
\left|u_6\left(t,R^1\right)-u_6\left(t,R^2\right)\right|^2 &= \left|-\rho\left(R^1-R^2\right)\right|^2\\
&\leq \left|\varepsilon_5^2+\rho^2\right|\left|R^1-R^2\right|^2\\
&= \bar{l}_6\left|R^1-R^2\right|^2.
\end{aligned}$$

Also, we write

$$\begin{aligned}
\left|C_1\left(t,S^1\right)-C_1\left(t,S^2\right)\right|^2 &= \sigma_1^2\left|S^1-S^2\right|^2 \leq \frac{3}{2}\sigma_1^2\left|S^1-S^2\right|^2,\\
\left|C_2\left(t,E^1\right)-C_2\left(t,E^2\right)\right|^2 &= \sigma_2^2\left|E^1-E^2\right|^2 \leq \frac{3}{2}\sigma_2^2\left|E^1-E^2\right|^2,\\
\left|C_3\left(t,V^1\right)-C_3\left(t,V^2\right)\right|^2 &= \sigma_3^2\left|V^1-V^2\right|^2 \leq \frac{3}{2}\sigma_3^2\left|V^1-V^2\right|^2,\\
\left|C_4\left(t,I^1\right)-C_4\left(t,I^2\right)\right|^2 &= \sigma_4^2\left|I^1-I^2\right|^2 \leq \frac{3}{2}\sigma_4^2\left|I^1-I^2\right|^2,\\
\left|C_5\left(t,Q^1\right)-C_5\left(t,Q^2\right)\right|^2 &= \sigma_5^2\left|Q^1-Q^2\right|^2 \leq \frac{3}{2}\sigma_5^2\left|Q^1-Q^2\right|^2,\\
\left|C_6\left(t,R^1\right)-C_6\left(t,R^2\right)\right|^2 &= \sigma_6^2\left|R^1-R^2\right|^2 \leq \frac{3}{2}\sigma_6^2\left|R^1-R^2\right|^2.
\end{aligned}$$

Then, we can conclude that the system has a unique solution [3].

3.2. **Numerical Analysis of a Stochastic Measles Model Using Newton Polynomial Method.** In this subsection, numerical algorithm based on Newton polynomial approach [3] will be presented for stochastic measles model with Caputo fractional derivative. In order to do this, we can facilitate the system (3.1) as

$$\begin{aligned}
{}_0^C D_t^\alpha S(t) &= f_1(S,E,V,I,Q,R,t)+\sigma_1 S(t)\,dB_1(t),\\
{}_0^C D_t^\alpha E(t) &= f_2(S,E,V,I,Q,R,t)+\sigma_2 E(t)\,dB_2(t),\\
{}_0^C D_t^\alpha V(t) &= f_3(S,E,V,I,Q,R,t)+\sigma_3 V(t)\,dB_3(t),\\
{}_0^C D_t^\alpha I(t) &= f_4(S,E,V,I,Q,R,t)+\sigma_4 I(t)\,dB_4(t),\\
{}_0^C D_t^\alpha Q(t) &= f_5(S,E,V,I,Q,R,t)+\sigma_5 Q(t)\,dB_5(t),\\
{}_0^C D_t^\alpha R(t) &= f_6(S,E,V,I,Q,R,t)+\sigma_6 R(t)\,dB_6(t).
\end{aligned} \tag{3.2}$$

To address discrepancies associated with the time dimension between the left- and right-hand sides of the equations, the right-hand side of the corrected system corresponding to the model in (3.2) is expressed as follows [6]:

$$\begin{aligned}
f_1(S,E,V,I,Q,R,t) &= \omega^\alpha+\tau^\alpha V-\left(b^\alpha+\rho^\alpha+\beta^\alpha I\right)S,\\
f_2(S,E,V,I,Q,R,t) &= \beta^\alpha IS-\left(\rho^\alpha+\mu^\alpha\right)E,\\
f_3(S,E,V,I,Q,R,t) &= b^\alpha S-\left(\rho^\alpha+\tau^\alpha\right)V,\\
f_4(S,E,V,I,Q,R,t) &= \mu^\alpha E-\left(\psi^\alpha+\rho^\alpha+\eta^\alpha+\theta^\alpha\right)I,\\
f_5(S,E,V,I,Q,R,t) &= \eta^\alpha I-\left(c^\alpha+\rho^\alpha+\delta^\alpha\right)Q,\\
f_6(S,E,V,I,Q,R,t) &= \theta^\alpha I+\delta^\alpha Q-\rho^\alpha R.
\end{aligned}$$

Applying the Caputo integral for $t=t_{n+1}$ to the system (3.2), we get the following

$$\begin{aligned}
S(t_{n+1}) &= \frac{1}{\Gamma(\alpha)}\left[\int_0^{t_{n+1}}(t_{n+1}-\tau)^{\alpha-1}f_1(S,E,V,I,Q,R,\tau)\,d\tau+\int_0^{t_{n+1}}(t_{n+1}-\tau)^{\alpha-1}\sigma_1 S(\tau)\,dB_1(\tau)\right],\\
E(t_{n+1}) &= \frac{1}{\Gamma(\alpha)}\left[\int_0^{t_{n+1}}(t_{n+1}-\tau)^{\alpha-1}f_2(S,E,V,I,Q,R,\tau)\,d\tau+\int_0^{t_{n+1}}(t_{n+1}-\tau)^{\alpha-1}\sigma_2 E(\tau)\,dB_2(\tau)\right],\\
V(t_{n+1}) &= \frac{1}{\Gamma(\alpha)}\left[\int_0^{t_{n+1}}(t_{n+1}-\tau)^{\alpha-1}f_3(S,E,V,I,Q,R,\tau)\,d\tau+\int_0^{t_{n+1}}(t_{n+1}-\tau)^{\alpha-1}\sigma_3 V(\tau)\,dB_3(\tau)\right],\\
I(t_{n+1}) &= \frac{1}{\Gamma(\alpha)}\left[\int_0^{t_{n+1}}(t_{n+1}-\tau)^{\alpha-1}f_4(S,E,V,I,Q,R,\tau)\,d\tau+\int_0^{t_{n+1}}(t_{n+1}-\tau)^{\alpha-1}\sigma_4 I(\tau)\,dB_4(\tau)\right],
\end{aligned}$$

$$Q(t_{n+1}) = \frac{1}{\Gamma(\alpha)}\left[\int_0^{t_{n+1}} (t_{n+1}-\tau)^{\alpha-1} f_5(S,E,V,I,Q,R,\tau)\,d\tau + \int_0^{t_{n+1}} (t_{n+1}-\tau)^{\alpha-1}\sigma_5 Q(\tau)\,dB_5(\tau)\right],$$

$$R(t_{n+1}) = \frac{1}{\Gamma(\alpha)}\left[\int_0^{t_{n+1}} (t_{n+1}-\tau)^{\alpha-1} f_6(S,E,V,I,Q,R,\tau)\,d\tau + \int_0^{t_{n+1}} (t_{n+1}-\tau)^{\alpha-1}\sigma_3 R(\tau)\,dB_6(\tau)\right].$$

The above can be arranged as follows

$$S(t_{n+1}) = \frac{1}{\Gamma(\alpha)}\left[\sum_{k=2}^{n}\int_{t_k}^{t_{k+1}} (t_{n+1}-\tau)^{\alpha-1} f_1(S,E,V,I,Q,R,\tau)\,d\tau + \sum_{k=2}^{n}\int_{t_k}^{t_{k+1}} (t_{n+1}-\tau)^{\alpha-1}\sigma_1 S(\tau)\,dB_1(\tau)\right],$$

$$E(t_{n+1}) = \frac{1}{\Gamma(\alpha)}\left[\sum_{k=2}^{n}\int_{t_k}^{t_{k+1}} (t_{n+1}-\tau)^{\alpha-1} f_2(S,E,V,I,Q,R,\tau)\,d\tau + \sum_{k=2}^{n}\int_{t_k}^{t_{k+1}} (t_{n+1}-\tau)^{\alpha-1}\sigma_2 E(\tau)\,dB_2(\tau)\right],$$

$$V(t_{n+1}) = \frac{1}{\Gamma(\alpha)}\left[\sum_{k=2}^{n}\int_{t_k}^{t_{k+1}} (t_{n+1}-\tau)^{\alpha-1} f_3(S,E,V,I,Q,R,\tau)\,d\tau + \sum_{k=2}^{n}\int_{t_k}^{t_{k+1}} (t_{n+1}-\tau)^{\alpha-1}\sigma_3 V(\tau)\,dB_3(\tau)\right],$$

$$I(t_{n+1}) = \frac{1}{\Gamma(\alpha)}\left[\sum_{k=2}^{n}\int_{t_k}^{t_{k+1}} (t_{n+1}-\tau)^{\alpha-1} f_4(S,E,V,I,Q,R,\tau)\,d\tau + \sum_{k=2}^{n}\int_{t_k}^{t_{k+1}} (t_{n+1}-\tau)^{\alpha-1}\sigma_4 I(\tau)\,dB_4(\tau)\right],$$

$$Q(t_{n+1}) = \frac{1}{\Gamma(\alpha)}\left[\sum_{k=2}^{n}\int_{t_k}^{t_{k+1}} (t_{n+1}-\tau)^{\alpha-1} f_5(S,E,V,I,Q,R,\tau)\,d\tau + \sum_{k=2}^{n}\int_{t_k}^{t_{k+1}} (t_{n+1}-\tau)^{\alpha-1}\sigma_5 Q(\tau)\,dB_5(\tau)\right],$$

$$R(t_{n+1}) = \frac{1}{\Gamma(\alpha)}\left[\sum_{k=2}^{n}\int_{t_k}^{t_{k+1}} (t_{n+1}-\tau)^{\alpha-1} f_6(S,E,V,I,Q,R,\tau)\,d\tau + \sum_{k=2}^{n}\int_{t_k}^{t_{k+1}} (t_{n+1}-\tau)^{\alpha-1}\sigma_6 R(\tau)\,dB_6(\tau)\right].$$

We approximate the functions $f_i(\tau,S,E,V,I,Q,R)$, $i=1,...,6$ within the interval $[t_k,t_{k+1}]$ using the Newton polynomial [3]

$$\begin{aligned} P_k^i(\tau) &= f_i(t_{k-2},S_{k-2},E_{k-2},V_{k-2},I_{k-2},Q_{k-2},R_{k-2}) + \\ &+ \frac{f_i(t_{k-1},S_{k-1},E_{k-1},V_{k-1},I_{k-1},Q_{k-1},R_{k-1}) - f_i(t_{k-2},S_{k-2},E_{k-2},V_{k-2},I_{k-2},Q_{k-2},R_{k-2})}{\Delta t}(\tau - t_{k-2}) \\ &\quad f_i(t_k,S_k,E_k,V_k,I_k,Q_k,R_k) \\ &+ \frac{-2f_i(t_{k-1},S_{k-1},E_{k-1},V_{k-1},I_{k-1},Q_{k-1},R_{k-1}) + f_i(t_{k-2},S_{k-2},E_{k-2},V_{k-2},I_{k-2},Q_{k-2},R_{k-2})}{2(\Delta t)^2} \\ &\times(\tau - t_{k-2})(\tau - t_{k-1}), \quad \text{where } k \geq 2. \end{aligned}$$

Now, let us replace the functions f_1, f_2, f_3, f_4, f_5 and f_6 with their Newton polynomials and than using some routine operations [3], the following scheme can be constructed

$$
\begin{aligned}
S\left(t_{n+1}\right) &= \frac{(\Delta t)^{\alpha}}{\Gamma(\alpha+1)} \sum_{k=2}^{n} f_1\left(S^{k-2}, E^{k-2}, V^{k-2}, I^{k-2}, Q^{k-2}, R^{k-2}, t_{k-2}\right) A_1 \\
&+ \frac{(\Delta t)^{\alpha}}{\Gamma(\alpha+2)} \sum_{k=2}^{n} \begin{bmatrix} f_1\left(S^{k-1}, E^{k-1}, V^{k-1}, I^{k-1}, Q^{k-1}, R^{k-1}, t_{k-1}\right) \\ -f_1\left(S^{k-2}, E^{k-2}, V^{k-2}, I^{k-2}, Q^{k-2}, R^{k-2}, t_{k-2}\right) \end{bmatrix} A_2 \\
&+ \frac{(\Delta t)^{\alpha}}{2\Gamma(\alpha+3)} \sum_{k=2}^{n} \begin{bmatrix} f_1\left(S^{k}, E^{k}, V^{k}, I^{k}, Q^{k}, R^{k}, t_{k}\right) \\ +f_1\left(S^{k-2}, E^{k-2}, V^{k-2}, I^{k-2}, Q^{k-2}, R^{k-2}, t_{k-2}\right) \\ -2f_1\left(S^{k-1}, E^{k-1}, V^{k-1}, I^{k-1}, Q^{k-1}, R^{k-1}, t_{k-1}\right) \end{bmatrix} A_3 \\
&+ \frac{(\Delta t)^{\alpha-1}}{\Gamma(\alpha+1)} \sigma_1 \sum_{k=0}^{n} S\left(c_1\right)\left(B_1\left(t_{k+1}\right) - B_1\left(t_k\right)\right)\left((k+1)^{\alpha} - k^{\alpha}\right), \\
E\left(t_{n+1}\right) &= \frac{(\Delta t)^{\alpha}}{\Gamma(\alpha+1)} \sum_{k=2}^{n} f_2\left(S^{k-2}, E^{k-2}, V^{k-2}, I^{k-2}, Q^{k-2}, R^{k-2}, t_{k-2}\right) A_1 \\
&+ \frac{(\Delta t)^{\alpha}}{\Gamma(\alpha+2)} \sum_{k=2}^{n} \begin{bmatrix} f_2\left(S^{k-1}, E^{k-1}, V^{k-1}, I^{k-1}, Q^{k-1}, R^{k-1}, t_{k-1}\right) \\ -f_2\left(S^{k-2}, E^{k-2}, V^{k-2}, I^{k-2}, Q^{k-2}, R^{k-2}, t_{k-2}\right) \end{bmatrix} A_2 \\
&+ \frac{(\Delta t)^{\alpha}}{2\Gamma(\alpha+3)} \sum_{k=2}^{n} \begin{bmatrix} f_2\left(S^{k}, E^{k}, V^{k}, I^{k}, Q^{k}, R^{k}, t_{k}\right) \\ +f_2\left(S^{k-2}, E^{k-2}, V^{k-2}, I^{k-2}, Q^{k-2}, R^{k-2}, t_{k-2}\right) \\ -2f_2\left(S^{k-1}, E^{k-1}, V^{k-1}, I^{k-1}, Q^{k-1}, R^{k-1}, t_{k-1}\right) \end{bmatrix} A_3 \\
&+ \frac{(\Delta t)^{\alpha-1}}{\Gamma(\alpha+1)} \sigma_2 \sum_{k=0}^{n} E\left(c_2\right)\left(B_2\left(t_{k+1}\right) - B_2\left(t_k\right)\right)\left((k+1)^{\alpha} - k^{\alpha}\right), \\
V\left(t_{n+1}\right) &= \frac{(\Delta t)^{\alpha}}{\Gamma(\alpha+1)} \sum_{k=2}^{n} f_3\left(S^{k-2}, E^{k-2}, V^{k-2}, I^{k-2}, Q^{k-2}, R^{k-2}, t_{k-2}\right) A_1 \\
&+ \frac{(\Delta t)^{\alpha}}{\Gamma(\alpha+2)} \sum_{k=2}^{n} \begin{bmatrix} f_3\left(S^{k-1}, E^{k-1}, V^{k-1}, I^{k-1}, Q^{k-1}, R^{k-1}, t_{k-1}\right) \\ -f_3\left(S^{k-2}, E^{k-2}, V^{k-2}, I^{k-2}, Q^{k-2}, R^{k-2}, t_{k-2}\right) \end{bmatrix} A_2 \\
&+ \frac{(\Delta t)^{\alpha}}{2\Gamma(\alpha+3)} \sum_{k=2}^{n} \begin{bmatrix} f_3\left(S^{k}, E^{k}, V^{k}, I^{k}, Q^{k}, R^{k}, t_{k}\right) \\ +f_3\left(S^{k-2}, E^{k-2}, V^{k-2}, I^{k-2}, Q^{k-2}, R^{k-2}, t_{k-2}\right) \\ -2f_3\left(S^{k-1}, E^{k-1}, V^{k-1}, I^{k-1}, Q^{k-1}, R^{k-1}, t_{k-1}\right) \end{bmatrix} A_3 \\
&+ \frac{(\Delta t)^{\alpha-1}}{\Gamma(\alpha+1)} \sigma_3 \sum_{k=0}^{n} V\left(c_3\right)\left(B_3\left(t_{k+1}\right) - B_3\left(t_k\right)\right)\left((k+1)^{\alpha} - k^{\alpha}\right), \\
I\left(t_{n+1}\right) &= \frac{(\Delta t)^{\alpha}}{\Gamma(\alpha+1)} \sum_{k=2}^{n} f_4\left(S^{k-2}, E^{k-2}, V^{k-2}, I^{k-2}, Q^{k-2}, R^{k-2}, t_{k-2}\right) A_1 \\
&+ \frac{(\Delta t)^{\alpha}}{\Gamma(\alpha+2)} \sum_{k=2}^{n} \begin{bmatrix} f_4\left(S^{k-1}, E^{k-1}, V^{k-1}, I^{k-1}, Q^{k-1}, R^{k-1}, t_{k-1}\right) \\ -f_4\left(S^{k-2}, E^{k-2}, V^{k-2}, I^{k-2}, Q^{k-2}, R^{k-2}, t_{k-2}\right) \end{bmatrix} A_2 \\
&+ \frac{(\Delta t)^{\alpha}}{2\Gamma(\alpha+3)} \sum_{k=2}^{n} \begin{bmatrix} f_4\left(S^{k}, E^{k}, V^{k}, I^{k}, Q^{k}, R^{k}, t_{k}\right) \\ +f_4\left(S^{k-2}, E^{k-2}, V^{k-2}, I^{k-2}, Q^{k-2}, R^{k-2}, t_{k-2}\right) \\ -2f_4\left(S^{k-1}, E^{k-1}, V^{k-1}, I^{k-1}, Q^{k-1}, R^{k-1}, t_{k-1}\right) \end{bmatrix} A_3 \\
&+ \frac{(\Delta t)^{\alpha-1}}{\Gamma(\alpha+1)} \sigma_4 \sum_{k=0}^{n} I\left(c_4\right)\left(B_4\left(t_{k+1}\right) - B_4\left(t_k\right)\right)\left((k+1)^{\alpha} - k^{\alpha}\right),
\end{aligned}
$$

$$
\begin{aligned}
Q(t_{n+1}) = {} & \frac{(\Delta t)^{\alpha}}{\Gamma(\alpha+1)} \sum_{k=2}^{n} f_5\left(S^{k-2}, E^{k-2}, V^{k-2}, I^{k-2}, Q^{k-2}, R^{k-2}, t_{k-2}\right) A_1 \\
& + \frac{(\Delta t)^{\alpha}}{\Gamma(\alpha+2)} \sum_{k=2}^{n} \left[\begin{array}{c} f_5\left(S^{k-1}, E^{k-1}, V^{k-1}, I^{k-1}, Q^{k-1}, R^{k-1}, t_{k-1}\right) \\ -f_5\left(S^{k-2}, E^{k-2}, V^{k-2}, I^{k-2}, Q^{k-2}, R^{k-2}, t_{k-2}\right) \end{array} \right] A_2 \\
& + \frac{(\Delta t)^{\alpha}}{2\Gamma(\alpha+3)} \sum_{k=2}^{n} \left[\begin{array}{c} f_5\left(S^{k}, E^{k}, V^{k}, I^{k}, Q^{k}, R^{k}, t_{k}\right) \\ +f_5\left(S^{k-2}, E^{k-2}, V^{k-2}, I^{k-2}, Q^{k-2}, R^{k-2}, t_{k-2}\right) \\ -2f_5\left(S^{k-1}, E^{k-1}, V^{k-1}, I^{k-1}, Q^{k-1}, R^{k-1}, t_{k-1}\right) \end{array} \right] A_3 \\
& + \frac{(\Delta t)^{\alpha-1}}{\Gamma(\alpha+1)} \sigma_5 \sum_{k=0}^{n} Q(c_5) \left(B_5(t_{k+1}) - B_5(t_k)\right) \left((k+1)^{\alpha} - k^{\alpha}\right), \\
R(t_{n+1}) = {} & \frac{(\Delta t)^{\alpha}}{\Gamma(\alpha+1)} \sum_{k=2}^{n} f_6\left(S^{k-2}, E^{k-2}, V^{k-2}, I^{k-2}, Q^{k-2}, R^{k-2}, t_{k-2}\right) A_1 \\
& + \frac{(\Delta t)^{\alpha}}{\Gamma(\alpha+2)} \sum_{k=2}^{n} \left[\begin{array}{c} f_6\left(S^{k-1}, E^{k-1}, V^{k-1}, I^{k-1}, Q^{k-1}, R^{k-1}, t_{k-1}\right) \\ -f_6\left(S^{k-2}, E^{k-2}, V^{k-2}, I^{k-2}, Q^{k-2}, R^{k-2}, t_{k-2}\right) \end{array} \right] A_2 \\
& + \frac{(\Delta t)^{\alpha}}{2\Gamma(\alpha+3)} \sum_{k=2}^{n} \left[\begin{array}{c} f_6\left(S^{k}, E^{k}, V^{k}, I^{k}, Q^{k}, R^{k}, t_{k}\right) \\ +f_6\left(S^{k-2}, E^{k-2}, V^{k-2}, I^{k-2}, Q^{k-2}, R^{k-2}, t_{k-2}\right) \\ -2f_6\left(S^{k-1}, E^{k-1}, V^{k-1}, I^{k-1}, Q^{k-1}, R^{k-1}, t_{k-1}\right) \end{array} \right] A_3 \\
& + \frac{(\Delta t)^{\alpha-1}}{\Gamma(\alpha+1)} \sigma_6 \sum_{k=0}^{n} R(c_6) \left(B_6(t_{k+1}) - B_6(t_k)\right) \left((k+1)^{\alpha} - k^{\alpha}\right),
\end{aligned}
$$

where

$$
\begin{aligned}
A_1 &= (n-k+1)^{\alpha} - (n-k)^{\alpha}, \\
A_2 &= (n-k+1)^{\alpha}(n-k+3+2\alpha) - (n-k)^{\alpha}(n-k+3+3\alpha), \\
A_3 &= (n-k+1)^{\alpha}\left[2(n-k)^2 + (3\alpha+10)(n-k) + 2\alpha^2 + 9\alpha + 12\right] \\
&\quad - (n-k)^{\alpha}\left[2(n-k)^2 + (5\alpha+10)(n-k) + 6\alpha^2 + 18\alpha + 12\right],
\end{aligned}
$$

and $c_1, c_2, ..., c_6 \in [t_k, t_{k+1}]$.

It should be noted that the values of $S(t_1)$ and $S(t_2)$ must be calculated since the Newton polynomial requires three points for its construction. Clearly, the values of $S(t_1)$ and $S(t_2)$ can be obtained using the Euler and Adams–Bashforth methods. Accordingly, we have:

$$
S_1 = S_0 + \frac{h^{\alpha}}{\Gamma(\alpha+1)} f_1(t_0, S_0, E_0, V_0, I_0, Q_0, R_0)
$$

and

$$
S_2 = S_1 + \frac{h^{\alpha}}{\Gamma(\alpha+2)} f_1(t_1, S_1, E_1, V_1, I_1, Q_1, R_1) - \frac{h^{\alpha}}{\Gamma(\alpha+2)} f_1(t_0, S_0, E_0, V_0, I_0, Q_0, R_0).
$$

It is worth noting that the similar procedure can be applied to the other state variables of the measles model.

3.3. **Numerical Simulations.** Simulations play a crucial role in understanding the dynamics of measles outbreaks and evaluating potential interventions. While analytical models provide valuable insights, simulations allow us to explore complex scenarios and capture the variability in disease spread that real-world data often present. By simulating different vaccination strategies, quarantine measures, and social behaviors, we can assess their impact on transmission rates and predict the outcomes of potential outbreaks. Simulations provide a powerful tool for testing hypotheses, optimizing public health policies, and guiding decision-makers in managing and controlling measles outbreaks more

effectively. To achieve our aim, we consider the following model:

$$
\begin{aligned}
{}_0^C D_t^\alpha S(t) &= \omega^\alpha + \tau^\alpha V - (b^\alpha + \rho^\alpha + \beta^\alpha I) S + \sigma_1 S(t)\, dB_1(t), \\
{}_0^C D_t^\alpha E(t) &= \beta^\alpha I S - (\rho^\alpha + \mu^\alpha) E + \sigma_2 E(t)\, dB_2(t), \\
{}_0^C D_t^\alpha V(t) &= b^\alpha S - (\rho^\alpha + \tau^\alpha) V + \sigma_3 V(t)\, dB_3(t), \\
{}_0^C D_t^\alpha I(t) &= \mu^\alpha E - (\psi^\alpha + \rho^\alpha + \eta^\alpha + \theta^\alpha) I + \sigma_4 I(t)\, dB_4(t), \\
{}_0^C D_t^\alpha Q(t) &= \eta^\alpha I - (c^\alpha + \rho^\alpha + \delta^\alpha) Q + \sigma_5 Q(t)\, dB_5(t), \\
{}_0^C D_t^\alpha R(t) &= \theta^\alpha I + \delta^\alpha Q - \rho^\alpha R + \sigma_6 R(t)\, dB_6(t).
\end{aligned}
$$

The following parameters and initial conditions proposed in [1] were used while performing the numerical simulations:

$$
\begin{aligned}
\omega = 0.029, \eta = 0.012, c = 0.083, \beta = 0.09091, \rho = 0.0078, \psi = 0.125, \\
\tau = 0.0017, b = 0.7, \theta = 0.14286, \delta = 0.023, \mu = 0.125, \sigma_1 = 0.1, \\
\sigma_2 = 0.02, \sigma_3 = 0.018, \sigma_4 = 0.016, \sigma_5 = 0.014, \sigma_1 = 0.012, S(0) = 1000, \\
E(0) = 50, V(0) = 20, I(0) = 5, Q(0) = 2, R(0) = 0.
\end{aligned}
$$

The numerical simulations for each class of the measles model are depicted in Figures 1-6. It is important to emphasize that the time scale adopted in the simulations was set to "days."

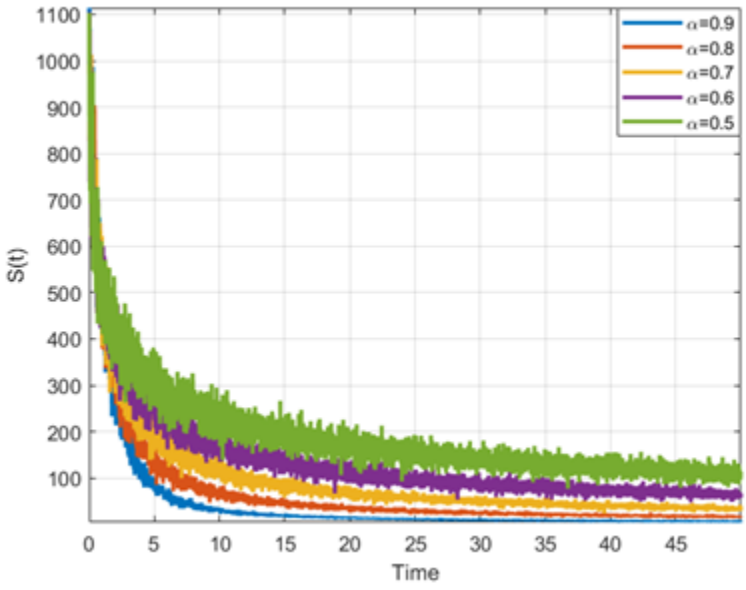

FIGURE 1. The visualization of the function $S(t)$ for different fractional orders.

Figure 1 shows the evolution of the susceptible (S) population under different values of the fractional-order derivative α. As α increases (approaching 1), the dynamics of the system become more responsive and closer to classical models. For lower values of α, the memory effect is stronger, resulting in a slower decay of the susceptible population. This implies that fractional-order derivatives introduce a memory effect: past states influence the current rate of change. The results highlight how fractional dynamics can delay or smooth the depletion of susceptibles, offering a more flexible modeling approach that better reflects real-world epidemic persistence.

Figure 2 illustrates the behavior of the exposed (E) compartment for various fractional orders. As α decreases, the peak of the exposed population becomes lower and broader, indicating that individuals move more slowly from the exposed to infected class. This reflects the fact that lower fractional orders introduce longer memory, effectively increasing the incubation-like effect in the system.

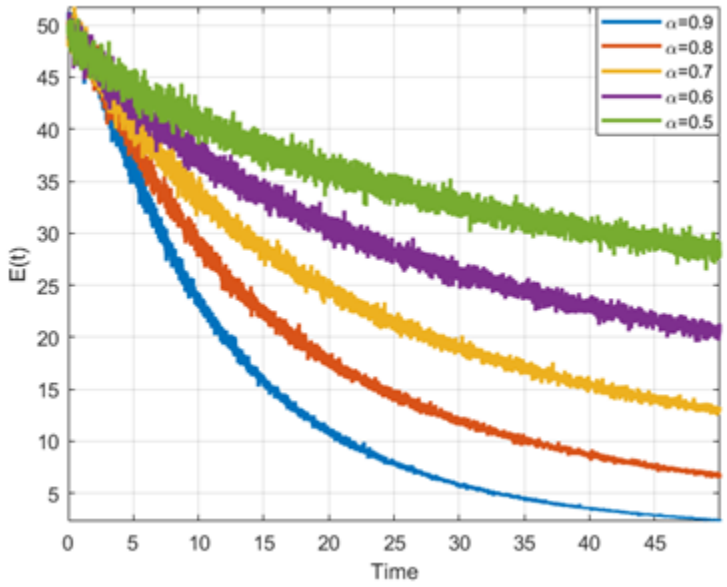

FIGURE 2. The visualization of the function $E(t)$ for different fractional orders.

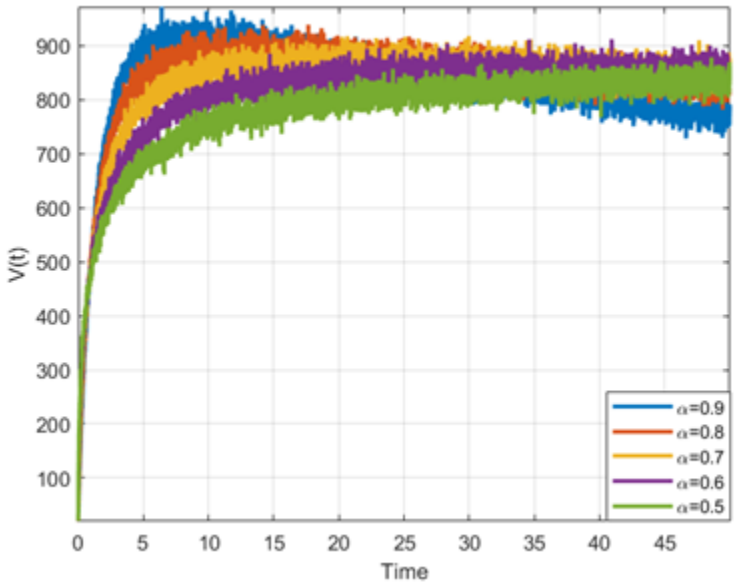

FIGURE 3. The visualization of the function $V(t)$ for different fractional orders.

Figure 3 shows the dynamics of the vaccinated population (V) under varying fractional orders α. When α is smaller, the growth in the number of vaccinated individuals is slower, showing how memory effects can dampen or delay the vaccination process—this may reflect realistic logistical delays or behavioral hesitancy. Higher α values lead to a quicker rise in V, resembling more immediate vaccination rollouts. The difference in curves highlights how the fractional-order derivative allows for flexible modeling of vaccination campaigns, including time-lagged effects and population response inertia.

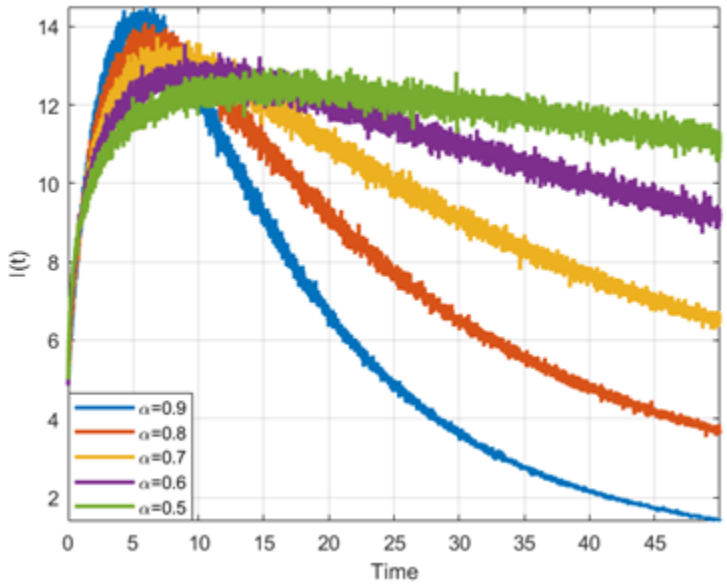

FIGURE 4. The visualization of the function $I(t)$ for different fractional orders.

Figure 4 focuses on the infected (I) population over time. A clear pattern emerges: for lower α values, the infection peaks are delayed and reduced in amplitude, while for higher α values, the outbreaks are sharper and occur sooner. This indicates that the memory effect associated with fractional calculus dampens and delays epidemic outbreaks. The stochastic nature of the model adds variability around each curve, but the general trend remains consistent.

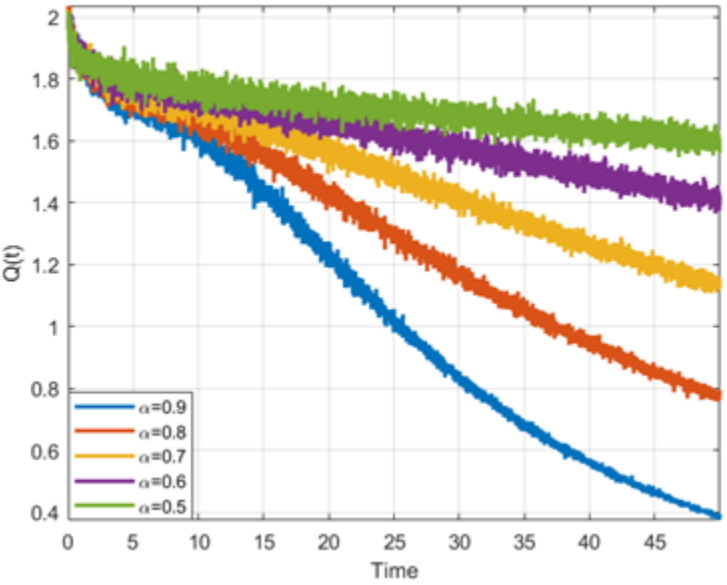

FIGURE 5. The visualization of the function $Q(t)$ for different fractional orders.

Figure 5 illustrates how the number of quarantined individuals (Q) evolves over time for different values of the fractional derivative α. For lower α values (e.g., $\alpha = 0.7$), the quarantined population increases more slowly and peaks later, reflecting the influence of memory effects in delaying transitions. As α approaches 1, the curve becomes sharper and the peak occurs earlier, indicating more immediate response dynamics typical of classical models. These trends suggest that fractional dynamics can better simulate delayed detection and isolation patterns in epidemics, particularly in real-life scenarios where quarantine implementation may lag behind infection spread.

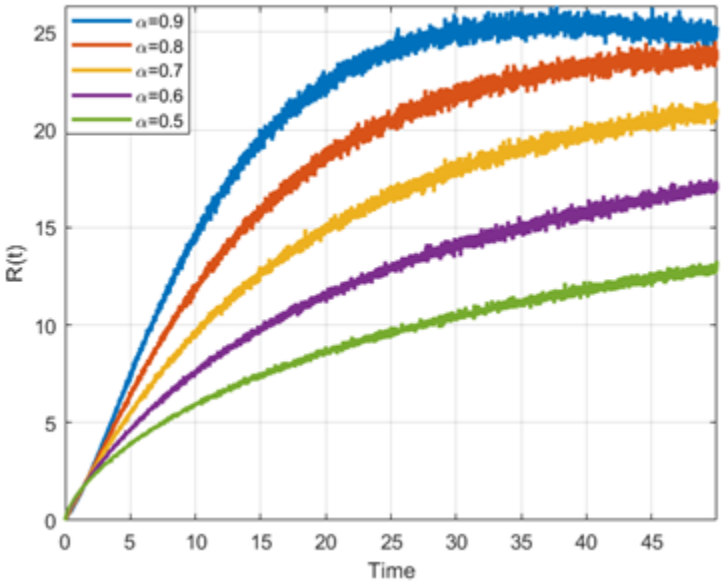

FIGURE 6. The visualization of the function $R(t)$ for different fractional orders.

Figure 6 depicts the evolution of the recovered population (R) across different fractional orders α. At lower α values, the recovery process is significantly delayed and more gradual, a consequence of the system's memory retaining past infection states longer. As α increases toward 1, the recovery curve rises more steeply, reflecting faster disease resolution in a classical framework.

4. Discussion and Future Directions

This section delves into the stochastic behavior of the fractional-order measles model by examining the dynamics of each compartment under varying values of the fractional derivative order, α. Figures 1-6 provide a detailed visualization of how memory effects, introduced through fractional calculus, influence the temporal evolution of the susceptible (S), exposed (E), vaccinated (V), infected (I), quarantined (Q), and recovered (R) populations. These figures not only underscore the flexibility and realism imparted by fractional derivatives but also reveal how the order α functions as a key control parameter for examining process in each compartment. The impact of the fractional order is clearly observed in the time evolution of each variable. For lower values of α, the system exhibits stronger memory effects, leading to slower transitions and delayed peaks across all compartments. In Figure 1, the susceptible population decreases more gradually with smaller α, indicating a delayed depletion due to slower disease progression. Figure 2 shows that the exposed population builds up and declines more slowly under strong memory, reflecting a prolonged incubation period. Figure 3 depicts the vaccination process, where lower α values lead to a slower uptake of vaccinated individuals, possibly modeling public response inertia or logistical constraints. Figure 4 reveals that infections rise and fall more sluggishly for lower α, with reduced and delayed peaks—an essential feature for capturing realistic epidemic delays. Figure 5 demonstrates that the quarantined population reaches its maximum later and more gently for smaller α, highlighting how memory effects can mimic real-world delays in detection and isolation. Lastly, Figure 6 shows that the accumulation of recovered individuals is more gradual for smaller α, illustrating how fractional dynamics

effectively capture prolonged recovery behaviors. Overall, the figures collectively emphasize that the fractional order α serves as a crucial tuning parameter, controlling the memory and responsiveness of each epidemiological process and enhancing the model's ability to replicate real-world disease dynamics under uncertainty.

Now, we present simulations to evaluate the behavior of some state variables in the measles model under different values of the parameters η (the rate at which infected individuals are isolated) and b (the rate at which susceptible individuals are vaccinated).

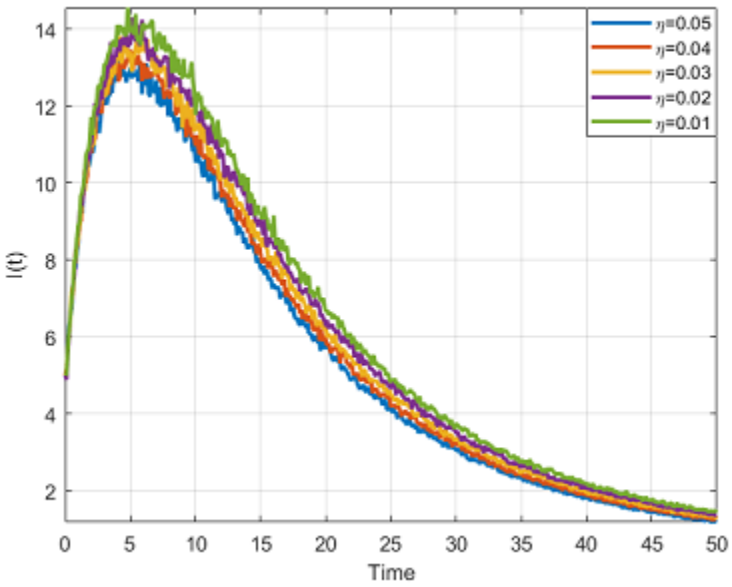

FIGURE 7. Time evolution of the infected population $I(t)$ under varying isolation rates η.

Figure 7 presents the progression of the infected population $I(t)$ over time across varying isolation rate values η. Higher isolation rates (larger η) lead to lower and earlier peaks in the infected population, indicating effective containment of the outbreak through timely quarantine. Conversely, lower values of η result in a delayed and intensified peak due to slower removal of infectious individuals.

Figure 8 illustrates how the quarantined population $Q(t)$ changes over time for different isolation rates η. As η increases, more individuals are moved into quarantine more rapidly, leading to higher and earlier peaks in $Q(t)$. Lower η values correspond to less efficient isolation, resulting in smaller and delayed peaks in the quarantined population.

Figure 9 depicts the changes in the vaccinated population $V(t)$ for different values of the vaccination rate b. Higher values of b significantly accelerate the accumulation of vaccinated individuals and raise the peak vaccination level, reflecting the impact of intensified immunization strategies. Lower vaccination rates cause a slower and more limited rise in the vaccinated population.

Figure 10 illustrates how the infected population $I(t)$ evolves over time under varying vaccination rates b. Increasing the vaccination rate b significantly reduces the infected population $I(t)$ by decreasing both the peak and total number of infections. High vaccination rates lead to earlier and smaller outbreaks, while low rates result in delayed and larger infection peaks. This emphasizes the importance of timely and widespread vaccination in controlling the epidemic.

Future work can address these limitations by incorporating data-driven parameter fitting techniques, considering heterogeneous or age-structured populations, and extending the model to incorporate fractional operators with other kernels, such as the Atangana-Baleanu type. Additionally, optimal control strategies, sensitivity analysis, and comparison with real epidemiological data could further validate the model's practical utility. Expanding the stochastic framework to include adaptive noise intensity or coupling with agent-based models could also enhance realism. Overall, this work lays the foundation for more robust and realistic epidemic forecasting models, especially in settings with limited data or high uncertainty.

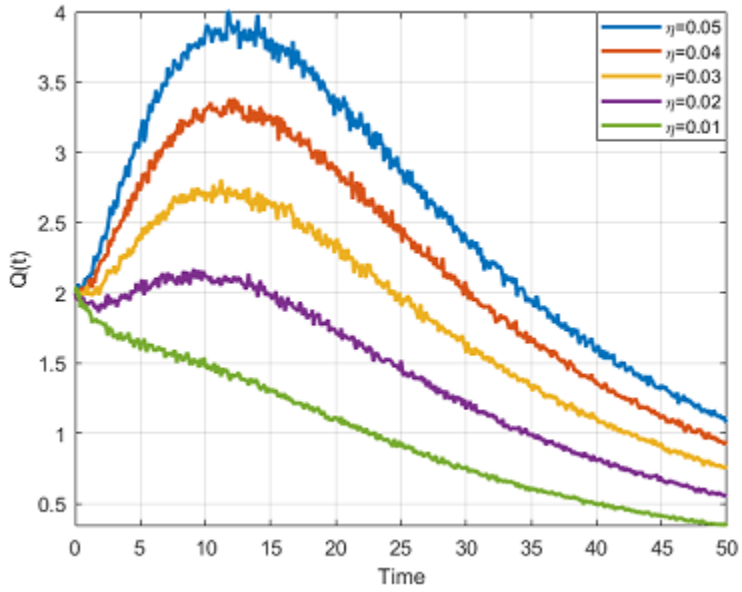

FIGURE 8. Time evolution of the quarantined population $Q(t)$ for different values of the isolation rate η.

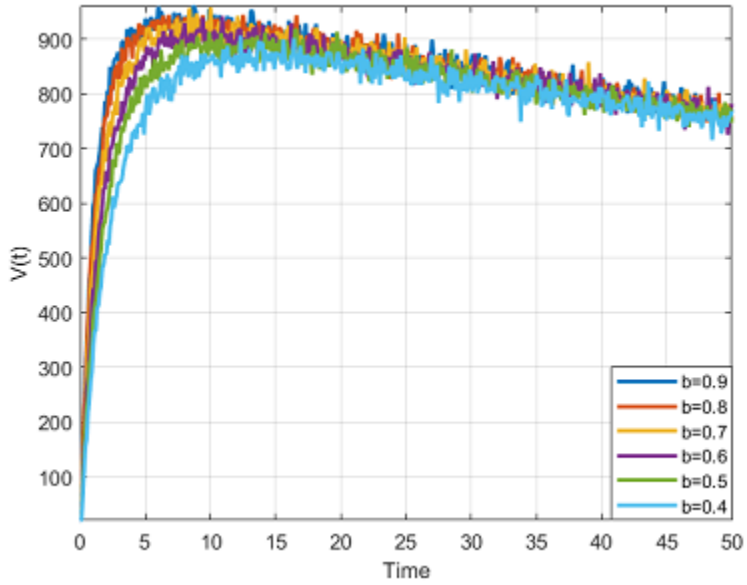

FIGURE 9. Dynamics of the vaccinated population $V(t)$ over time for various vaccination rates b.

5. CONCLUSION

This study successfully investigates the dynamics of a measles infection model by integrating stochastic frameworks with the Caputo fractional derivative. The inclusion of fractional-order calculus introduces memory-dependent behavior into the system, allowing the model to capture complex temporal patterns—such as delayed responses, prolonged

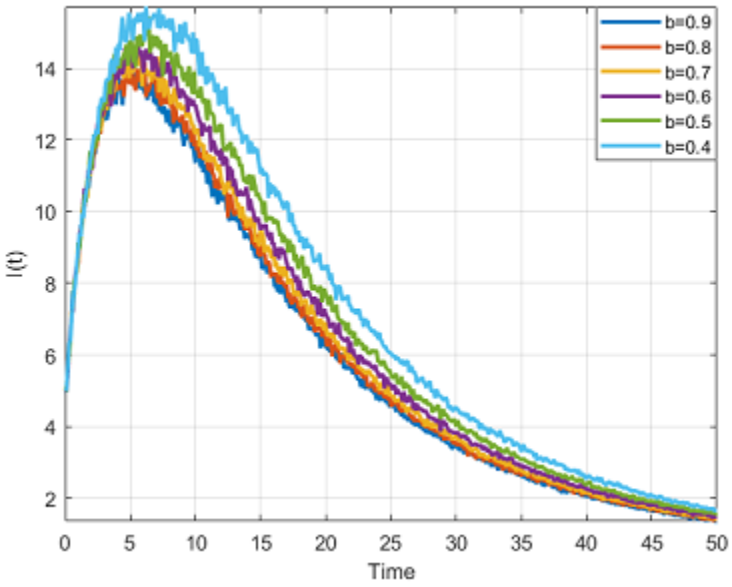

FIGURE 10. Dynamics of the vaccinated population $I(t)$ over time for various vaccination rates b.

infectious periods, and gradual recovery—that are often overlooked by traditional integer-order models. Through rigorous mathematical analysis, the existence and uniqueness of the solution were established using linear growth and Lipschitz conditions, ensuring the theoretical soundness of the model.

Numerical simulations, performed via the Newton polynomial method, efficiently approximate the model's behavior under various fractional orders for all epidemiological compartments (S, E, V, I, Q, R). The results underscore the significance of incorporating stochastic dynamics. In particular, the stochastic component offers a more realistic depiction of real-world epidemics by accounting for uncertainties such as random contacts, behavioral variability, and reporting inconsistencies.

A major novelty of this work lies in its hybrid approach that combines nonlocal fractional dynamics with stochastic modeling, offering a more flexible and robust framework for infectious disease analysis. This approach not only enhances theoretical understanding but also provides practical insights for understanding epidemic diseases. Furthermore, the model paves the way for future research by demonstrating how fractional derivatives can be employed to study other infectious diseases or extended to more complex systems with heterogeneous structures or alternative kernels. Overall, this study establishes a strong foundation for advancing epidemiological modeling under uncertainty and memory effects.

ACKNOWLEDGEMENT

We sincerely thank the reviewers and editors for their valuable comments and suggestions, which have significantly improved the clarity, depth, and quality of our manuscript.

CONFLICTS OF INTEREST

The author/authors declare that there are no conflicts of interest regarding the publication of this article.

AUTHORS CONTRIBUTION STATEMENT

Mehmet Akif Çetin: Conceptualization, Investigation; Visualization; Roles/Writing - original draft; Writing - review, editing. **Seda İğret Araz**: Conceptualization, Investigation, Methodology, Software, Visualization, Writing - review, editing. All authors discussed the results and contributed to the final manuscript.

References

[1] Akuka, P.N.A., Seidu, B., Okyere, E., Abagna, S., *Fractional-order Epidemic model for Measles infection*, Scientifica, **2024**(2024).

[2] Arık, I.A., Sarı H.K., Igret Araz S., *Numerical simulation of Covid-19 model with integer and non-integer order: The effect of environment and social distancing*, Results in Physics, **51**(2023).

[3] Atangana, A., İgret Araz, S., Fractional Stochastic Differential Equations: Applications to Covid-19 Modeling, Springer Nature, Singapore, 2022.

[4] Boubekeur, M.A., Bel hamiti, O., *Modelling of obesity impact on COVID-19: Improved SEIR model*, Mathematical Foundations of Computing, (2025).

[5] Caputo, M., *Linear model of dissipation whose Q is almost frequency independent II*, Geo-physical Journal International, **13**(1967), 529–539.

[6] Diethelm, K. *A fractional calculus based model for the simulation of an outbreak of dengue fever*, Nonlinear Dynamics, **71**(2013), 613–619.

[7] İğret Araz, S., Boulaaras, S., *Fractional modeling of gradual incorporation of infected prey into the predator-prey system with consideration of seasonality*, Applied Mathematics in Science and Engineering, **33**(2025).

[8] Ma, J., Ma, Z., *Epidemic threshold conditions for seasonally forced SEIR models*, Mathematical Biosciences & Engineering, **3**(2006).

[9] Miskovic-Stankovic, V., Janev, M., Atanackovic, T.M.. *Two compartmental fractional derivative model with general fractional derivative*,Journal of Pharmacokinetics and Pharmacodynamics, **50**(2023), 79–87.

[10] Momoh, A.A., Ibrahim, M.O., Uwanta, I.J., Manga, S.B., *Mathematical model for control of measles epidemiology*, International Journal of Pure and Applied Mathematics, **87**(2013).

[11] Peter, O.J., Afolabi, O.A., Victor, A.A., Akpan, C.E. , Oguntolu, F.A., *Mathematical model for the control of measles*, Journal of Applied Sciences and Environmental Management, **22**(2018), 571–576.

[12] Satsuma, J., Willox, R., Ramani, A., Grammaticos, B., Carstea, A.S., *Extending the SIR epidemic model*, Physica A: Statistical Mechanics and its Applications, **336**(2004).

[13] Shaikh, A.S., Shaikh, I.N., Nisar, K.S., *A mathematical model of COVID-19 using fractional derivative: outbreak in India with dynamics of transmission and control*, Advances in Difference Equations, **373**(2020).

[14] Thompson, K.M., *Evolution and use of dynamic transmission models for Measles and Rubella risk and policy analysis*, Risk Analysis, **36**(2016).

[15] Traore, A., Sene, N., *Model of economic growth in the context of fractional derivative*, Alexandria Engineering Journal, **59**(2020).